JOURNAL OF MATERIALS SCIENCE 15 (1980) 2636–2642

The mechanism of failure in bending of paperboard

LEIF CARLSSON, CHRISTER FELLERS, ALF DE RUVO
Swedish Forest Products Research Laboratory, Box 5604, S-114 86 Stockholm, Sweden

The behaviour of paperboard beams subjected to pure bending is analysed and related to tensile and compression stress–strain behaviour. Since the compression strength is lower than the tensile strength, beam failure occurs in compression. However, beam failure does not occur when the ultimate strain in pure compression is reached in the surface fibres. A plastic yielding in compression, which gives good agreement between experimentally-determined and theoretically-calculated bending moments up to failure is therefore suggested. At failure, the elastic energy stored in the sample causes propagation of an interlaminar crack at the compression side, which is observed in scanning electron micrographs.

1. Introduction

The success of paperboard as a rigid packaging material depends to a large extent on its unique property of being able to be converted to boxes by bending of the flat material along well-defined zones. These zones, consisting of delaminated layers, are achieved in the scoring operation, where a combination of bending and interlaminar shear causes the necessary reduction in the moment required to achieve bending [1].

In order to provide an insight into the basic mechanisms of the bending and scoring operations, the effects of interlaminar shear [2, 3] and pure bending must be studied separately.

The object of this study was to investigate, using scanning electron microscope (SEM) techniques, the failure mechanism in bending of homogeneous paperboards made from unbleached and bleached chemical pulps, and to relate the bending behaviour to the uniaxial tension and compression properties.

2. General background

The mechanism of failure of beams in bending has been described for many types of materials. Of special interest in this context is the failure mechanism of wood and fibre-reinforced composite materials.

Jenkin [4] investigated wood beams and observed visible lines of failure on the compression side of the beams. These lines, being a consequence of failure in compression, increase and extend down the beam cross-section as a larger moment is applied. This continues until the stress on the tension side reaches its ultimate value, when fracture occurs. Schniewind [5] showed that the maximum moment could be predicted from uniaxial tensile and compression strengths by consideration of a similar failure mechanism. The same mechanism of failure in bending of composite materials consisting of unidirectional aramid fibres in an epoxy matrix has been proposed by Zweben [6], who used the three-point bending test to predict the ultimate tensile stress from measured values of the maximum moment. A reasonably good prediction was obtained if the volume dependence of strength for brittle materials was incorporated into the theory. Thus in both wood and composite beams, the failure mechanism involves beam failure in tension, despite a lower strength in compression than in tension. In an investigation of single Kevlar fibres, Greenwood and Rose [7] proposed an alternative mechanism of failure in bending. In this case no tensile fracture occurred, but extensive buckling on the compression side of the fibre appeared during bending, and this was considered to be the cause of the fibre failure.

0022–2461/80/102636–07 $02.70/0

3. Theoretical considerations

If the tensile strength of a material is the same as the compression strength, the moment at failure in bending is merely another measure of the strength [8].

This is not true for paperboard. Furthermore, in order to calculate the relation between the bending moment and the curvature of paperboard, the strongly non-linear appearance of the stress–strain curves in tension and compression must also be taken into account.

The theory of pure bending of beams, when the material does not obey Hooke's law, may be formulated if it is assumed that cross-sections initially plane and normal to the neutral surface remain so after bending, and that the strain perpendicular to the neutral surface is negligible. These assumptions have been shown by Bach and Baumann [9] to be valid for materials exhibiting non-linear stress–strain behaviour.

Consider a cross-section of a paperboard beam subjected to bending as shown in Fig. 1. In order to determine the variation of strain and stress over the cross-section at different curvatures, the stress–strain curve of the material in tension and compression must be known. Furthermore, the following equations expressing equilibria of forces and moments must be used in order to calculate the moment:

$$\int \sigma dz = 0; \quad (1)$$

$$\int \sigma z \, dz = M, \quad (2)$$

where σ is the stress, z is the coordinate measured from the neutral surface and M is the bending moment.

In order to calculate the moments at various curvatures corresponding to the plastic region of the stress–strain curve, a numerical solution of Equations 1 and 2 has been derived (see Appendix 1). In order to achieve this, the stress–strain curve is inserted in a computer program which calculates the moment and curvature for each value of the compressive strain in the extreme fibres on the concave side of the beam, using Equations A9 and A6 in the Appendix.

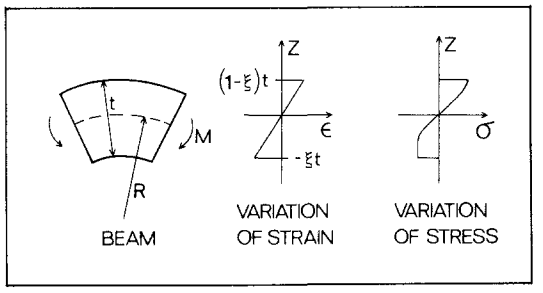

Figure 1 Variation of strain and stress over the cross-section.

4. Preparation of test samples and evaluation of properties

Orientated sheets of weight per unit area $110\,g\,m^{-2}$ were formed in a Formette Dynamique sheet former [10] using unbleached and bleached chemical pulps prepared in 56 and 47% yields (kg paper/kg wood) respectively.

Boards of weight per unit area $440\,g\,m^{-2}$ were made by couching and wet-pressing four $110\,g\,m^{-2}$ sheets. The boards were pressed at the same pressure and slowly dried to final moisture content equilibrium (23° C, 50% relative humidity) in drying frames to minimize gradients in elastic modulus through the thickness due to differences in drying rate, and to prevent shrinkage in both the MD and CD [11].

The stress–strain properties in tension and compression were evaluated in a specially designed apparatus [12] and the bending curves in a device developed for measuring pure bending properties of paper [13]. The density, measured by a mercury immersion technique described by Wasser [14], was $590\,kg\,m^{-3}$ and $700\,kg\,m^{-3}$ for the unbleached and bleached boards, respectively.

Samples, which had been bent to different curvatures, were kept in the curved state by gluing the edge of the beams to a piece of paperboard so that the surface could be studied by SEM-techniques in the curved state.

5. Results

Two different orientated homogeneous boards of weight per unit area $440\,g\,m^{-2}$, made in the laboratory from unbleached and bleached chemical pulps, were investigated by means of stress–strain curves, moment–curvature curves and scanning electron microscope (SEM) studies on the bent board beams.

5.1. Stress–strain curves

The stress–strain curves of the boards in the machine direction (MD) and cross-machine direc-

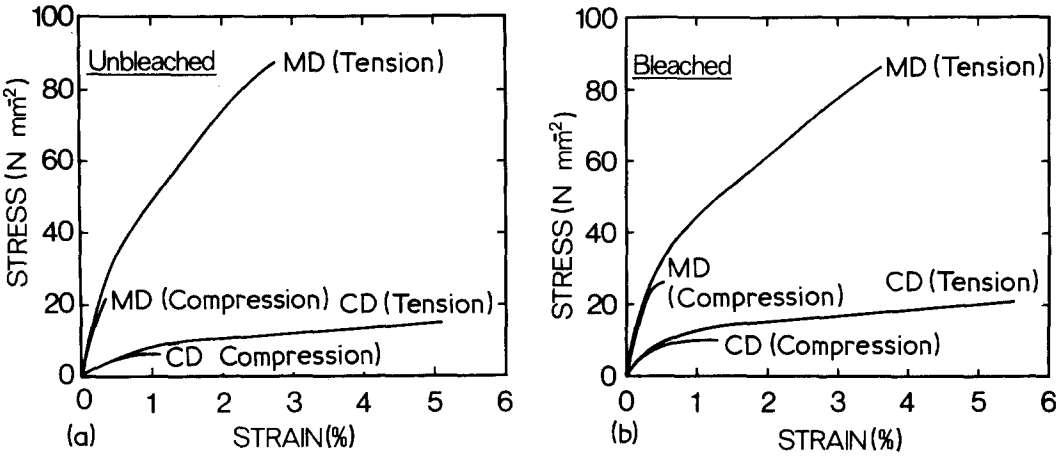

Figure 2 Stress–strain curves in tension and compression for boards made from (a) unbleached and (b) bleached chemical pulps, respectively.

tion (CD) were obtained in tension and compression and are given in Fig. 2. In agreement with earlier studies of the compression behaviour [15, 16], it is noted that the compression and tension elastic moduli are equal and that the ultimate stress and the strain to failure are much lower in the compression mode than in the tension mode.

The appearance of compressive failure is shown in Fig. 3. Earlier investigations [15, 16] have shown that failure in compression is caused by local instabilities in the fibre wall. The release of elastic energy finally results in the gross out-of-plane dislocation shown in Fig. 3.

5.2. Moment–curvature curves

Moment–curvature curves for the board beams, shown in Fig. 4, were obtained in both the MD and the CD. Analogous to the stress–strain curves in tension and compression, the initial slope of the curves represents the bending stiffness and the maximum moment represents the bending strength.

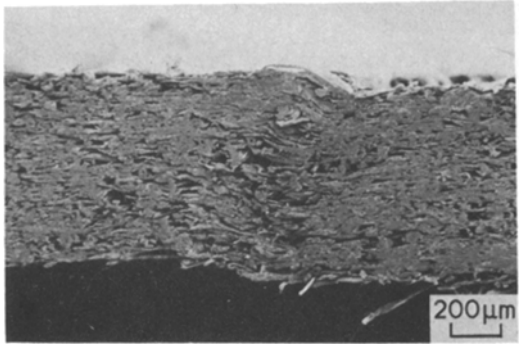

Figure 3 SEM-micrograph of the compression failure zone.

The bending strength in the MD is reached at moderate curvature and is followed by a pronounced moment drop, while the moment–curvature curves in the CD are horizontal over a considerable curvature range after the bending strength is reached. No moment decrease could be detected within practical limits of bending in this direction.

Samples at three characteristic curvatures were chosen for SEM-studies as indicated in Fig. 4. The circles represent the curvature where the strain-to-failure in pure compression is reached in the surface fibres on the compression side (calculated from Equation A6, the triangles represent a curvature close to the point where the maximum moment is reached and the squares represent a curvature after the maximum moment is reached. It should be noted that the samples were kept in the curved state during the SEM-studies.

5.3. Failure mechanism in bending

From a consideration of the stress–strain curves in Fig. 2, it would be expected that beam failure would occur in compression since the compression strength is lower than the tensile strength. This hypothesis is confirmed in Fig. 5, which shows representative SEM-photographs of the edge of unbleached board beams bent to failure (squares in Fig. 4). The bleached board showed the same failure appearance. It is evident (Fig. 5) that no tensile fracture occurred, and that the beam failure must be attributed to a compression failure.

It may be observed in the photographs that interlaminar crack-propagation has occurred on

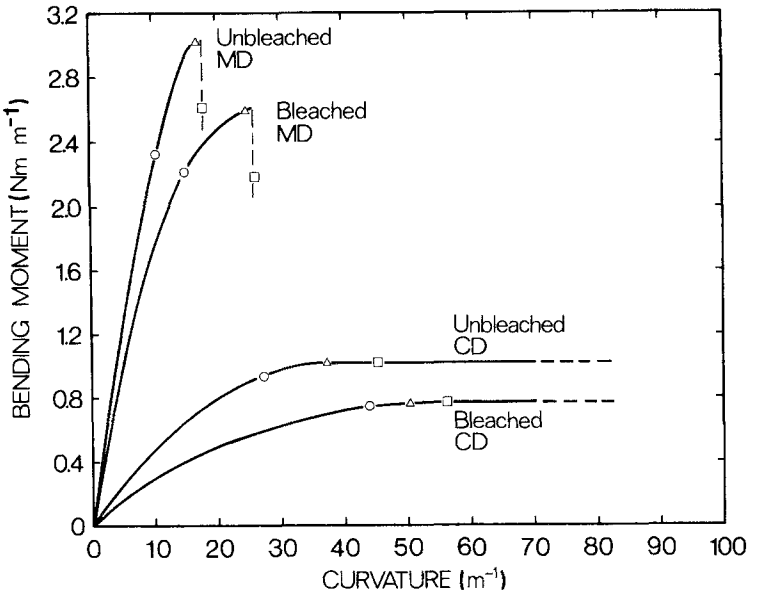

Figure 4 Bending moment–curvature curves for the boards.

the compression side, which has resulted in an out-of-plane displacement of several fibre layers. The main difference between the MD and CD beams is a more pronounced delamination in the MD beam, and this explains the marked decrease in bending moment when failure occurs in this direction.

Beam failure did not occur immediately at the curvature where the strain-to-failure in pure compression was reached in the surface fibres, as indicated by circles in the moment–curvature curves in Fig. 4. Instead, both the moment and curvature increased beyond this point. This behaviour was further investigated by SEM-studies.

Fig. 6 shows a representative part of the concave, compressed surface at the point of maximum moment in the MD and CD (triangles in Fig. 4) for the unbleached board. Again, the bleached board showed the same appearance as the unbleached board. The deformations of the surface fibres appear as small dislocations of the fibre walls and buckling of fibres on the segmental level. It was also observed that fewer fibre wall dislocations and buckled fibres were present in the concave compressed surface at the point of strain-to-failure in pure compression (circles in Fig. 4) than at the maximum moment.

In order to clarify whether any interlaminar crack propagation occurs prior to beam failure, the compression strength, which is a sensitive indicator of any local delamination of the structure, was measured for beams previously bent to different curvatures and then submitted to a compression test. Fig. 7 shows the compression strength for beams which had been bent to different curvatures divided by the compression strength for unbent beams. It may be noted that the compression strength remains unchanged up to a certain curvature and then drastically drops. This

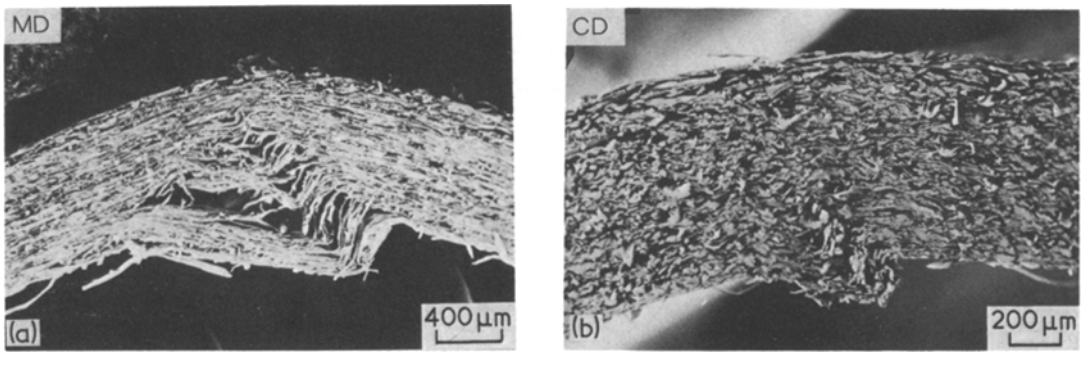

Figure 5 SEM-micrographs of the edges of paperboard beams in the MD and CD bent to failure.

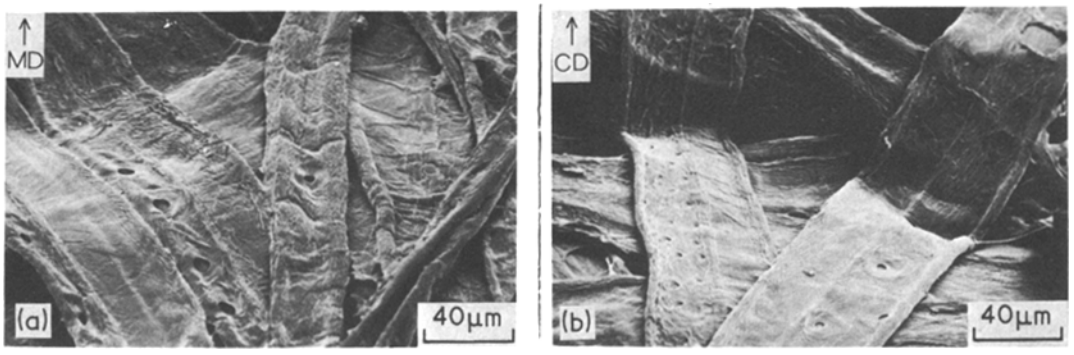

Figure 6 SEM-micrographs of the concave, compressed surface of bent paperboard beams in the MD and CD.

curvature corresponds to the curvature at the maximum moment in Fig. 4. Consequently no local delamination or interlaminar cracks were introduced in the structure prior to the curvature where the maximum moment is reached. The absence of local delamination before beam failure implies, analogous to the behaviour of wood beams, that the material begins to yield when the ultimate strain in pure compression is reached in the surface fibres.

To quantify the effect of yielding on the bending behaviour, Equations A6 and A9 were used, assuming that the yielding zone at constant ultimate compression stress penetrates the cross-section as the curvature increases. Fig. 8 shows that this assumption gives a good agreement with the experimental curves at all curvatures up to the maximum moment; with the error being less than 4%. The results thus provide evidence for the occurrence of a yielding behaviour on the compression side before the maximum moment is reached.

On the assumption that yielding occurs, the variation of stress through the thickness at the point-of-failure was calculated and is shown in Fig. 9. The portion of the cross-section subjected to constant compression stress is shown by a circle on the z-axis. This portion ranges between 10 and 25% of the thickness. The compression strain at the concave surface is approximately 50 to 100% greater than the strain-to-failure in pure compression. In addition, the neutral surface at the point of failure has moved from the centre of the beam towards the convex surface, a distance of approximately 5% of the thickness.

6. Conclusions

Beam failure does not occur when the ultimate strain in pure compression is reached in the surface fibres. By measuring the compression strength of beams which have been bent so that the strain of the compression surface has exceeded the strain-to-failure in pure compression it is demonstrated that no major flaws or interlaminar cracks have been introduced in the structure before beam failure occurs.

Evidently the structure, to a greater extent than in pure compression, maintains its integrity in the bending mode. This must be due to the stabilizing effect of the part of the beam stressed in tension

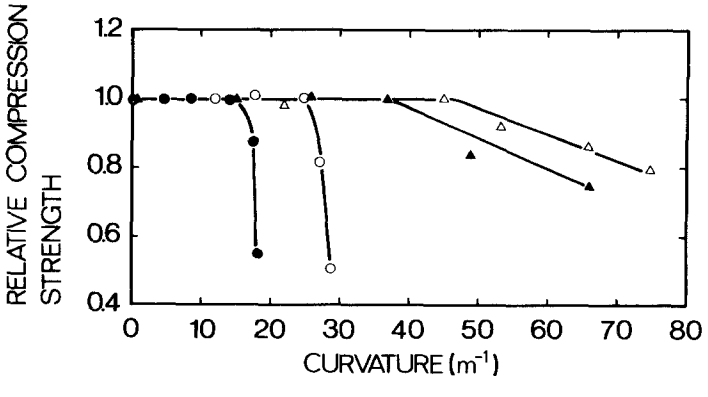

Figure 7 Relative compression strength for beams which had been bent to different curvatures. ● = Unbleached MD, ○ = Bleached MD, ▲ = Unbleached CD, △ = Bleached CD.

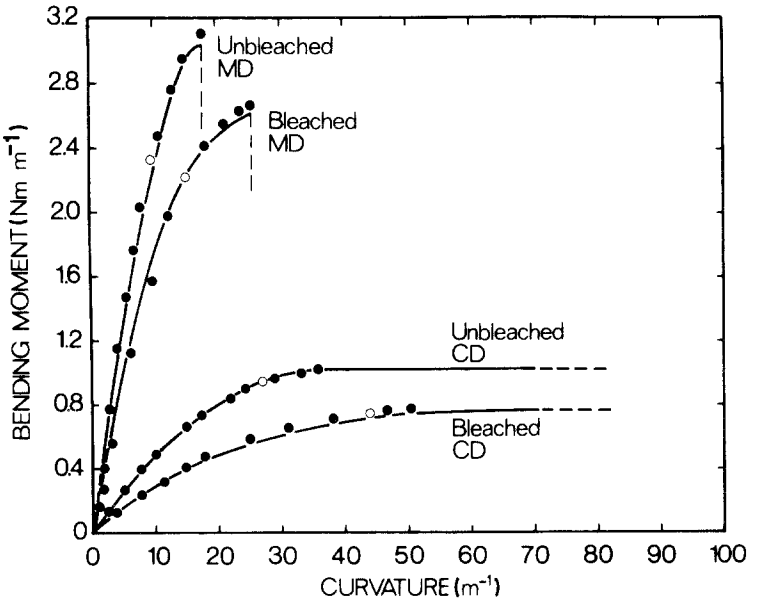

Figure 8 Measured curves and predicted values of bending moment versus curvature.

and the curved geometry of the beam which does not favour out-of-plane displacement of the compressed layers.

A plastic yielding in compression caused by yielding on the fibre wall level is therefore suggested. This hypothesis gives good agreement between experimentally-determined and theoretically-calculated moments up to failure.

At beam failure, fibre segments subjected to compressive deformations are forced out of the plane. Elastic energy, which is stored in the beam, is released and is consumed by the consequent propagation of an interlaminar crack. This results in the typical delaminated appearance of the fractured zones.

From the results of this investigation it may be anticipated that it is the interlaminar crack propagation resistance of the material which determines its fractographic appearance and the decrease in bending moment at failure. This property must consequently be considered important for the creasability of the board.

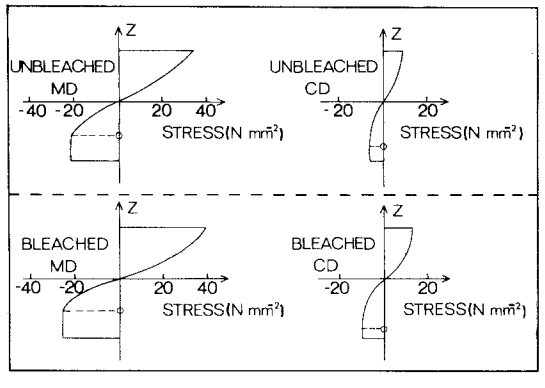

Figure 9 Variation of stress through the thickness at the point of failure in bending.

Appendix

The equilibrium of forces and moments is expressed by

$$\int \sigma dz = 0 \qquad \text{(A1)}$$

and

$$\int \sigma z dz = M. \qquad \text{(A2)}$$

The origin of the z co-ordinate is located at the neutral surface of the beam which is not, in general, located at the mid-depth of the beam. Therefore a parameter ξ is defined in accordance with Fig. 1, where the distances from the neutral surface to the compressed and extended surface fibres are, respectively, ξt and $(1-\xi)t$ where t is the thickness and $0 < \xi < 1$. Equation A1 then becomes

$$\int_0^{(1-\xi)t} \sigma dz = \int_0^{\xi t} \sigma dz, \qquad \text{(A3)}$$

where σ is the absolute value of the stress. Numerical solution of this equation enables the position of the neutral surface, i.e. the value of ξ, to be determined when the stress–strain curve is known. Applying the trapezium formula for the numerical

solution of integrals, Equation A3 may be expressed as

$$\Delta z_T \sum_{i=0}^{T-1} (\sigma_i + \sigma_{i+1}) = \Delta z_C \sum_{j=0}^{C-1} (\sigma_j + \sigma_{j+1}), \quad (A4)$$

where $\Delta z_T = (1 - \xi)t/T$, $\Delta z_C = \xi t/C$ and T and C are the number of thickness increments on the tension and compression side respectively. σ_i is the tensile stress ($i = 0, 1, \ldots T$) and σ_j is the compressive stress ($j = 0, 1, \ldots C$).

The variation of strain through the thickness is expressed by:

$$\epsilon = z/R, \quad (A5)$$

where R is the radius of curvature of the beam at the neutral surface (see Fig. 1). The calculations are based on a predetermined value ϵ_C of the compressive strain in the extreme fibres on the compression side of the beam. For a given value of ϵ_C the curvature $1/R$ is given by

$$\frac{1}{R} = \frac{\epsilon_C}{\xi t}. \quad (A6)$$

The tensile and compressive strains ϵ_i and ϵ_j, respectively, are calculated

$$\epsilon_i = i \cdot \Delta z_T/R \quad (i = 0, 1, \ldots T), \quad (A7)$$

$$\epsilon_j = j \cdot \Delta z_C/R \quad (j = 0, 1, \ldots C). \quad (A8)$$

The corresponding tensile and compression stresses σ_i and σ_j are obtained from the stress–strain curves.

Since the neutral surface is not in general located at the beam mid-depth, the correct position is obtained by an iterative procedure which continues until Equation A4 is fulfilled. Finally, the moment can be calculated by numerical solution of Equation A2

$$M = \frac{\Delta z_T^2}{2} \sum_{i=0}^{T-1} (i\sigma_i + (i+1)\sigma_{i+1}) + \frac{\Delta z_C^2}{2} \sum_{j=0}^{C-1} (j\sigma_j + (j+1)\sigma_{j+1}). \quad (A9)$$

Acknowledgement

The authors wish to thank Ms Berit Möllerberg for skilful experimental assistance. Thanks are also due to Dr Adrian Wallis for linguistic revision.

References

1. A. G. EMSLIE and R. S. BRENNEMAN, *Tappi* **50** (6) (1967) 289.
2. V. L. BYRD, V. C. SETTERHOLM and J. F. WICHMAN, *ibid.* **58** (10) (1975) 132.
3. C. FELLERS, *Svensk Papperstidn.* **80** (3) (1977) 89.
4. C. F. JENKIN, Report on materials of construction used in aircraft and aircraft engines, Great Britain Aeronautical Research Committee, 1920.
5. A. P. SCHNIEWIND, *Inst. of Wood Sci.* 9 (1962) 12.
6. C. ZWEBEN, *J. Composite Mater.* **12** (1978) 422.
7. J. H. GREENWOOD and P. C. ROSE, *J. Mater. Sci.* 9 (1974) 1809.
8. R. M. JONES, *J. Composite Mater.* **10** (1976) 342.
9. C. BACH and R. BAUMANN, "Elastizität und Festigkeit", 9th Edn., (Julius Springer, Berlin, 1924).
10. G. SAURET, H. J. TRINH and G. LETEBVRE, *Das Papier* **23** (1969) 8.
11. M. HTUN, to be published.
12. C. FELLERS, in "Handbook of Physical and Mechanical Testing of Paper and Paperboard", edited by R. E. Mark, to be published by Marcel Dekker, New York.
13. C. FELLERS and L. CARLSSON, *Tappi* **62** (8) (1979) 107.
14. R. B. WASSER, *ibid.* **57** (3) (1974) 166.
15. S. CAVLIN and C. FELLERS, *Svensk Papperstidn.* **78** (9) (1975) 329.
16. C. FELLERS, A. De RUVO, J. ELFSTRÖM and M. HTUN, *Tappi* **63** (6) (1980) 109.

Received 8 February and accepted 27 March 1980.